# A Convergence Study of Multimaterial Mesh-based Surface Tracking

Fang Da* Columbia University
Christopher Batty† University of Waterloo
Eitan Grinspun‡ Columbia University

## Abstract

We report the results from experiments on the convergence of the multimaterial mesh-based surface tracking method introduced by the same authors. Under mesh refinement, approximately first order convergence or higher in L1 and L2 is shown for vertex positions, face normals and non-manifold junction curves in a number of scenarios involving the new operations proposed in the method.[1]

**Keywords:**

## 1 Introduction

Multimaterial mesh-based surface tracking [Da et al. 2014] was proposed as an algorithm for tracking interfaces between multiple materials undergoing large and complex deformations and topological changes. This technical report summarizes the results of numerical experiments conducted to evaluate convergence of this tracking algorithm.

## 2 Method

We have performed convergence experiments to test the method's convergence properties under refinement of the mesh resolution. For each experiment, we perform a series of simulations, each with decreased upper and lower bounds on edge lengths compared to the previous one. We then measure the error by comparing the computed interface geometry against the analytical solution, or against the simulation of the highest resolution if no analytical solution is available. To compare two interfaces, we measure the deviation of the position, surface normals, and non-manifold junction curves between the computed interface and the reference solution, as detailed in the next section.

The initial configuration of every simulation in a given experiment is the same high-resolution input mesh. For lower resolution simulations, the algorithm rapidly adjusts this mesh to satisfy the target edge length bounds through remeshing. However, since the edge lengths in the simulation results are only confined to a range, doubling the edge length bounds generally won't exactly double the average edge length. Therefore, rather than use edge length bounds as our independent variable in plots of error vs. resolution, we instead use the mean edge length measured from the computed geometry.

*e-mail:fang@cs.columbia.edu
†e-mail:christopher.batty@uwaterloo.ca
‡e-mail:eitan@cs.columbia.edu

[1]Per the SIGGRAPH policy on double submission, **no aspect of this project has been submitted for publication elsewhere**, including this preliminary and unpublished technical report. We have included this report with our submission for reviewer reference.

The upper and lower bounds for the edge length during remeshing are set to 0.5 times and 1.5 times the target edge length for a given resolution, resulting in edge length distributions that typically resemble Figure 1, whose data was drawn from the merging experiment (see Section 4.1). In this case, the mean edge length is 0.00935 with a standard deviation of 0.00103.

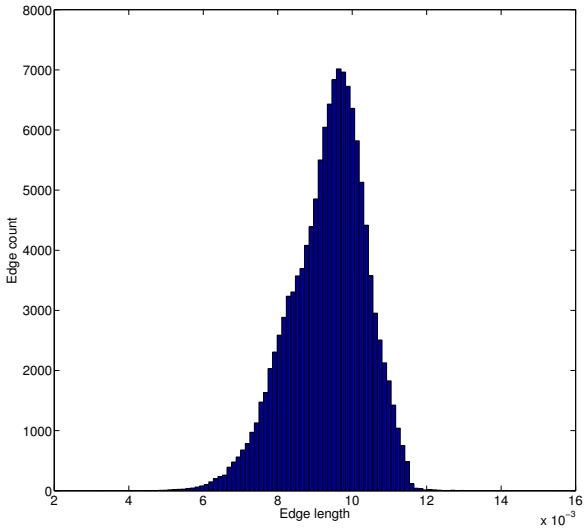


**Figure 1:** *Histogram of edge lengths for the first simulation in the merging experiment.*

### 2.1 Error descriptors for comparison between two meshes

**Notation** Each convergence experiment considers a reference solution and a sequence of trial solutions. The reference solution is represented by the reference mesh containing $\bar{N}$ vertices, $\bar{\mathbf{v}}_i$, and $\bar{M}$ triangular faces with corresponding surface normals $\bar{\mathbf{n}}_i$. A particular trial solution is represented by a test (or trial) mesh containing $N$ vertices $\mathbf{v}_i$ and $M$ faces with normals $\mathbf{n}_i$.

For every vertex $\bar{\mathbf{v}}_i$ on the reference mesh, its closest point $\mathbf{x}_i$ on the test mesh is found, and their Euclidean distance $\|\mathbf{x}_i - \bar{\mathbf{v}}_i\|$ is computed. We define the *position error 1-norm* and *2-norm* by

$$E_1^{\mathrm{p}} = \frac{1}{\bar{A}} \sum \bar{A}_i \|\mathbf{x}_i - \bar{\mathbf{v}}_i\| \quad (1)$$

and

$$E_2^{\mathrm{p}} = \sqrt{\frac{1}{\bar{A}} \sum \bar{A}_i \|\mathbf{x}_i - \bar{\mathbf{v}}_i\|^2} \quad (2)$$

where the discretized area $\bar{A}_i$ on vertex $\bar{\mathbf{v}}_i$ is computed by summing one third of each incident face's area, and $\bar{A}$ is the total area of the reference mesh.

For every face on the reference mesh, the closest face on the test mesh in terms of centroid distance is found, and the two-norm of

the difference between the unit normal $\bar{\mathbf{n}}_i$ of the reference mesh face and the unit normal $\mathbf{n}_i$ of the test mesh face is computed. We then compute the *normal error 1-norm* and *2-norm*

$$E_1^{\mathrm{n}} = \frac{1}{\bar{A}} \sum \bar{A}_i \|\mathbf{n}_i - \bar{\mathbf{n}}_i\|, \tag{3}$$

$$E_2^{\mathrm{n}} = \sqrt{\frac{1}{\bar{A}} \sum \bar{A}_i \|\mathbf{n}_i - \bar{\mathbf{n}}_i\|^2}, \tag{4}$$

respectively, where $\bar{A}_i$ refers to the area of the $i^{th}$ face.

We define the *junction vertex sets* $\bar{J}$ and $J$ (for the reference and trial mesh respectively) to be the set of vertices that are incident to at least three different materials. For every junction vertex $\bar{\mathbf{v}}_i \in \bar{J}$ on the reference mesh, the closest junction vertex $\mathbf{v}_i \in J$ on the test mesh is found and their Euclidean distance is computed. The *curve error 1-norm* and *2-norm* are computed from these, as

$$E_1^{\mathrm{c}} = \frac{1}{\bar{L}} \sum_{\bar{\mathbf{v}}_i \in \bar{J}} \bar{L}_i \|\mathbf{v}_i - \bar{\mathbf{v}}_i\|, \tag{5}$$

$$E_2^{\mathrm{c}} = \sqrt{\frac{1}{\bar{L}} \sum_{\bar{\mathbf{v}}_i \in \bar{J}} \bar{L}_i \|\mathbf{v}_i - \bar{\mathbf{v}}_i\|^2}, \tag{6}$$

respectively, where the discretized non-manifold curve length $\bar{L}_i$ on vertex $\bar{\mathbf{v}}_i$ is computed by summing one half of each incident non-manifold edge's length, and $\bar{L}$ is the total non-manifold curve length on the reference mesh.

### 2.2 Error descriptors for comparison between a mesh and an analytical solution

For cases where the solution can be expressed in closed form, we define an unsigned distance function $d^{\mathrm{p}}(\mathbf{x})$ as the distance from $\mathbf{x}$ to the closest point on the surface, and another unsigned distance function $d^{\mathrm{c}}(\mathbf{x})$ as the distance from $\mathbf{x}$ to the closest point on the network of junction curves, which is the subset of the interface that is incident to at least three different materials. Then we can compute the same error descriptors, this time indexing the summation over the test mesh:

$$E_1^{\mathrm{p}} = \frac{1}{A} \sum A_i d^{\mathrm{p}}(\mathbf{v}_i), \tag{7}$$

$$E_2^{\mathrm{p}} = \sqrt{\frac{1}{A} \sum A_i d^{\mathrm{p}}(\mathbf{v}_i)^2}, \tag{8}$$

$$E_1^{\mathrm{n}} = \frac{1}{A} \sum A_i \|\nabla d^{\mathrm{p}}(\mathbf{f}_i) - \mathbf{n}_i\|, \tag{9}$$

$$E_2^{\mathrm{n}} = \sqrt{\frac{1}{A} \sum A_i \|\nabla d^{\mathrm{p}}(\mathbf{f}_i) - \mathbf{n}_i\|^2}, \tag{10}$$

$$E_1^{\mathrm{c}} = \frac{1}{L} \sum L_i d^{\mathrm{c}}(\mathbf{c}_i), \tag{11}$$

$$E_2^{\mathrm{c}} = \sqrt{\frac{1}{L} \sum L_i d^{\mathrm{c}}(\mathbf{c}_i)^2}. \tag{12}$$

Here $\mathbf{f}_i$ is the centroid of the $i^{th}$ face.

## 3 A static equilibrium problem

We first test the convergence of the method in a manner that is independent of the particular time integration scheme, by examining the static equilibrium configuration of a simulation. Our first problem considers minimizers of surface tension energy subject to fixed material volumes. We consider two cubes of different materials, sharing a common face, immersed within a third ambient material. For the governing PDE we consider gradient descent along a surface tension potential with equal surface tension coefficient for all three interfaces, and a volume deviation penalty for each contiguous material region

$$\dot{\mathbf{x}} = -\gamma \nabla A - \eta \sum_{j=1}^{N_{\mathrm{region}}} (V_j - V_j^{\mathrm{init}}) \nabla V_j. \tag{13}$$

Here $A$ is the surface area of the mesh and $V_j$ is the volume of region $j$. The volume penalty stiffness $\eta$ is chosen sufficiently large to dominate the surface tension stiffness $\gamma$ (we used $\eta = 10^3$, $\gamma = 10^{-9}$) resulting in a much smaller error due to volume deviation than mesh discretization errors. We used a simple Forward Euler time integration scheme to evolve the PDE until it reached steady state.

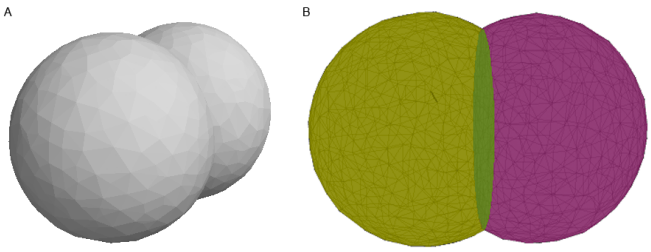


**Figure 2:** *The final geometry of the statics experiment. (A) flat shaded opaque view; (B) semi-transparent view with each color denoting a patch of interface.*

The final interface (a standard “double bubble") is shown in Figure 2. It is then compared to the analytical solution given by Hass and Schlafly [2000]. Figure 3 shows the various error descriptors plotted against the mean edge length. All error descriptors show at least first-order convergence.

## 4 Dynamic problems

Next we investigate the convergence of the method over dynamic simulations. Specifically, we consider the following three remeshing topology process that are proposed in the original paper [Da et al. 2014]: snapping-based mesh merging, T1 process, and T2 process. For each operation, an experiment is specifically designed to exercise that operation, and convergence is tested by examining the geometry at a fixed point in time after the operation has occurred.

### 4.1 Multimaterial mesh merging

The multimaterial merging operation is tested using a multimaterial normal flow scenario involving two expanding spheres of different materials, which is a straightforward extension of the two-phase experiment conducted by Brochu and Bridson [2009]. We consider two initially disjoint spheres enclosing different materials, both immersed within a third ambient material. The two spheres expand at unit speed in the outward normal direction using the *face offsetting method* [Jiao 2007]. In the analytical solution, the two spheres come into contact at time $t = 0.5$, and merging begins. This yields a new interface separating the two spheres, which is set to have zero velocity. As the simulation proceeds, this interface expands as a circular disc, resulting in a circular three-material junction curve. The geometries at $t = 0$ and $t = 1.8$ are shown in Figure 4. We

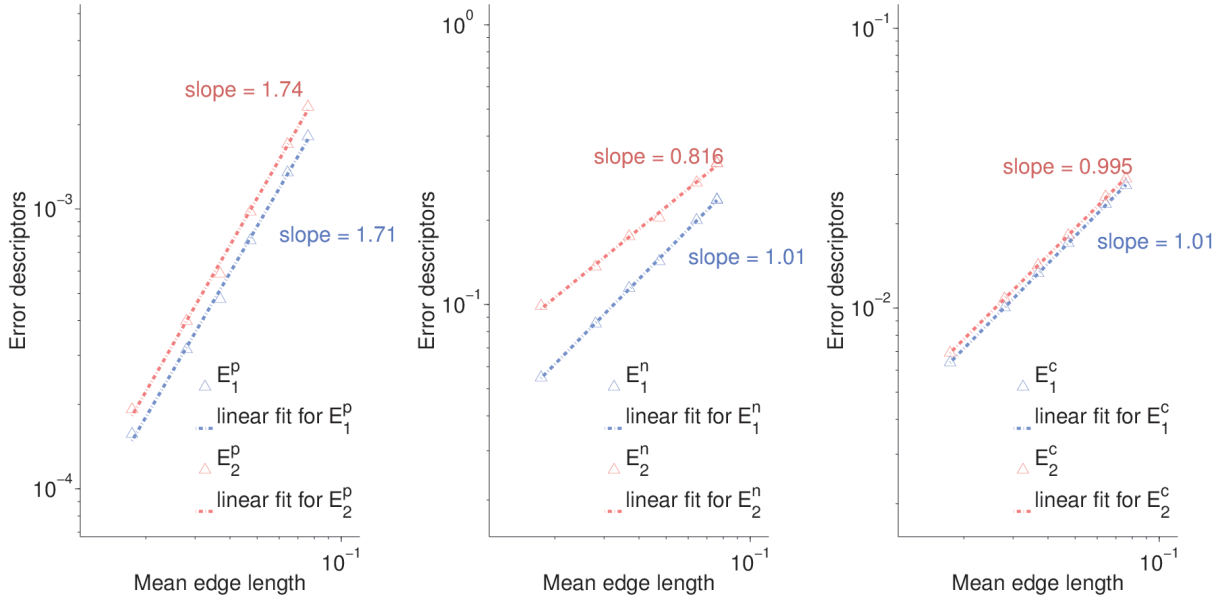


**Figure 3:** *Error vs. mean edge length for the statics experiment, for positions (left), normals (center) and triple-curves (right).*

compare the geometry at $t = 1.8$ to the analytical solution, and plot the error descriptors against mean edge length in Figure 5. All error descriptors show at least first-order convergence.

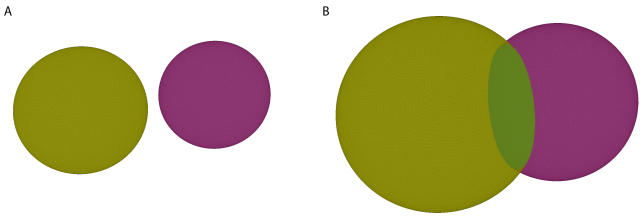


**Figure 4:** *The initial (A) and final (B) geometry off the two-sphere face offsetting experiment.*

### 4.2 T1 process

Our next experiment tests the vertex separation operation, which in combination with edge collapses allows a T1 process to occur. The initial geometry is a $\times$-shape extruded in the $z$ direction, as shown in Figure 6A. The velocity field is given by a time-invariant function $v(x, y, z) = [x, -y, 0]$. Crucially, this velocity field possesses a stagnation point with zero velocity along the entire z-axis, which coincides with the non-manifold junction. This is a challenging case because the analytical solution does *not* undergo a T1 process (as in the numerical result in Figure 6 C).

The surface tracking method under consideration resolves T1 processes by estimating a quantity termed the *separation strength*, a function of the flow behavior at irregular vertices. This separation strength can be computed either from the analytical velocity field, if it is available, or computed using local finite differences. The current test case illustrates a situation in which this choice can have an impact on the resulting geometry. Using the analytical separation strength, our algorithm correctly recovers the expected result shown Figure 6 C; since the velocity (and thus separation strength) is zero at that point, no vertex separation occurs and the quadruple junction remains as the mesh evolves. If instead we estimate the separation strength using finite differences from offset points along the potential separation directions (as may be more typical in simulation scenarios), the numerical separation strength is slightly *non-zero*. This leads to a vertex separation and the result in Figure 6 B. A small region near the irregular junction has separated, yielding a narrow horizontal strip whose size is proportional to the typical mesh edge length (essentially a numerical boundary layer). This is an artifact of the error in the finite difference estimate propagating to the surface tracking algorithm itself.

Nevertheless, this result is correct in a local integral sense, and the results indeed converge under refinement because the area of this region steadily shrinks. Figure 7 shows the results of this test case estimating separation strength via finite differences. The results were produced by comparing the mesh at a given time $t = 0.9$ (visualized in Figure 6 B) to the analytical solution, and plotting the error descriptors against mean edge length in Figure 7. All error descriptors show at least first-order convergence, with the exception of $E_2^n$; i.e., only the convergence of the surface normals in the $L2$ norm are impacted by the finite difference errors, and exhibit a slower convergence rate.

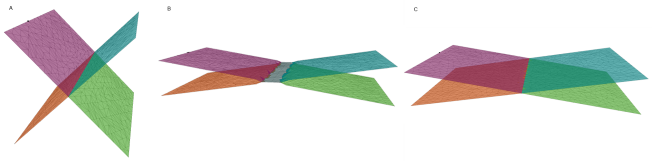

**Figure 6:** *The initial (A) and final (B) geometry of the T1 process experiment. (C) shows the final geometry when the user-supplied analytical velocity gradient is used instead of finite differencing in determining the separation tendency. Note that the non-manifold junction is not separated, which agrees with the analytical solution.*

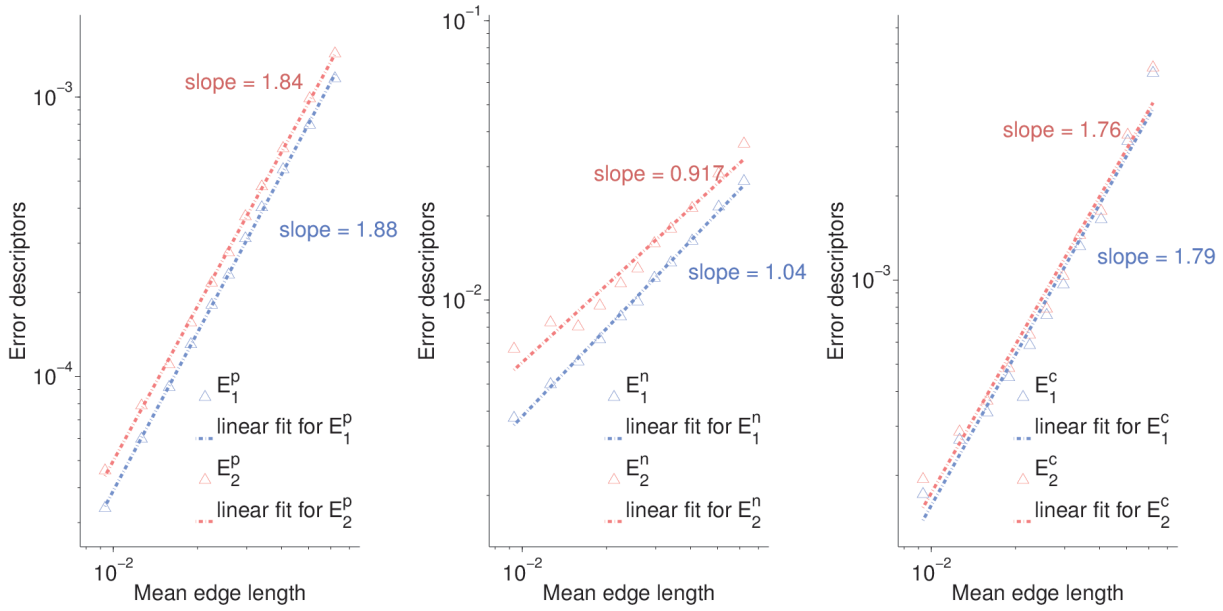


**Figure 5:** *Error vs. mean edge length for the two-sphere normal flow-induced merging experiment, for positions (left), normals (center) and triple-curves (right).*

### 4.3 T2 process

To test a T2 process, we consider mean curvature flow from an initial geometry consisting of a Reuleaux tetrahedron located at the junction of four planar Plateau borders (see Figure 8). The outer mesh boundary (at the intersection with the bounding cube) is fixed. Because the flat interfaces already meet at the optimal (equilibrium) angles, mean curvature flow simply reduces the size of the Reuleaux tetrahedron until it disappears. This completes the T2 process and produces a simple central vertex where four Plateau borders meet. We compare the geometry after the T2 process to the analytical solution, and plot the error descriptors against mean edge length in Figure 9. All error descriptors show at least first-order convergence.

## 5 Conclusions

The results from convergence experiments on the method are reported. Experiments involving various operations proposed in the multimaterial front tracking method [Da et al. 2014] demonstrate convergence under mesh refinement.

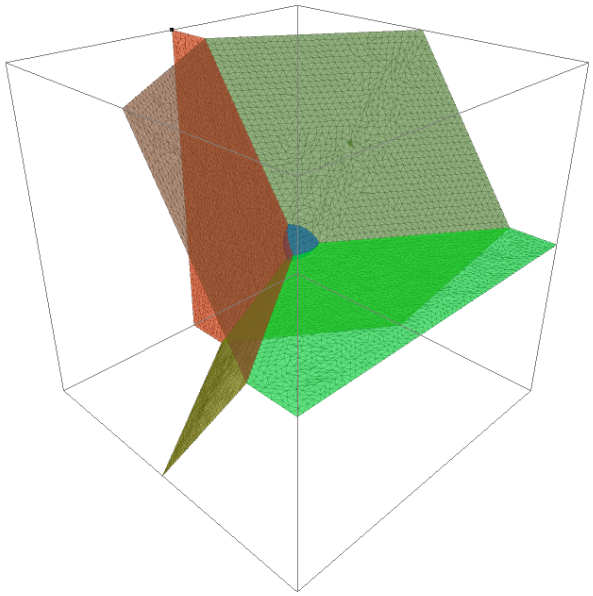

**Figure 8:** *The initial geometry of the Reuleaux tetrahedron experiment.*

## References


BROCHU, T., AND BRIDSON, R. 2009. Robust topological operations for dynamic explicit surfaces. *SIAM J. Sci. Comput. 31*, 4, 2472–2493.

DA, F., BATTY, C., AND GRINSPUN, E. 2014. Multimaterial mesh-based surface tracking. *ACM Trans. on Graphics (SIGGRAPH 2014)*.

HASS, J., AND SCHLAFLY, R. 2000. Double bubbles minimize. *Annals of Mathematics 151*, 459–515.

JIAO, X. 2007. Face offsetting: A unified approach for explicit moving interfaces. *J. Comp. Phys. 220*, 2, 612–625.

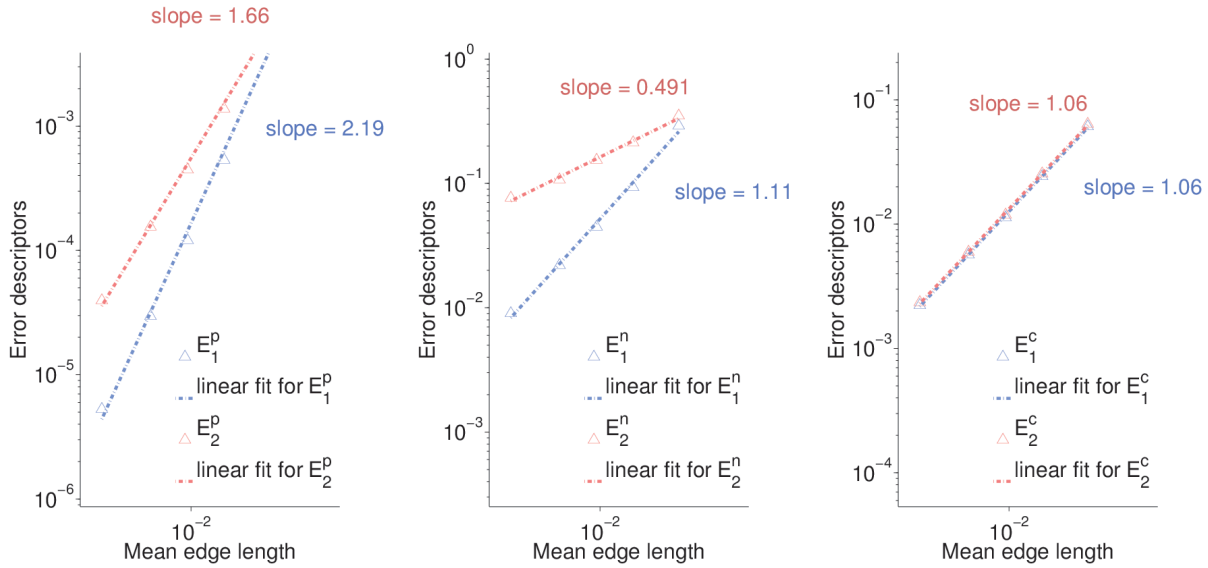


**Figure 7:** *Error vs. mean edge length for the T1 process experiment, for positions (left), normals (center) and triple-curves (right).*

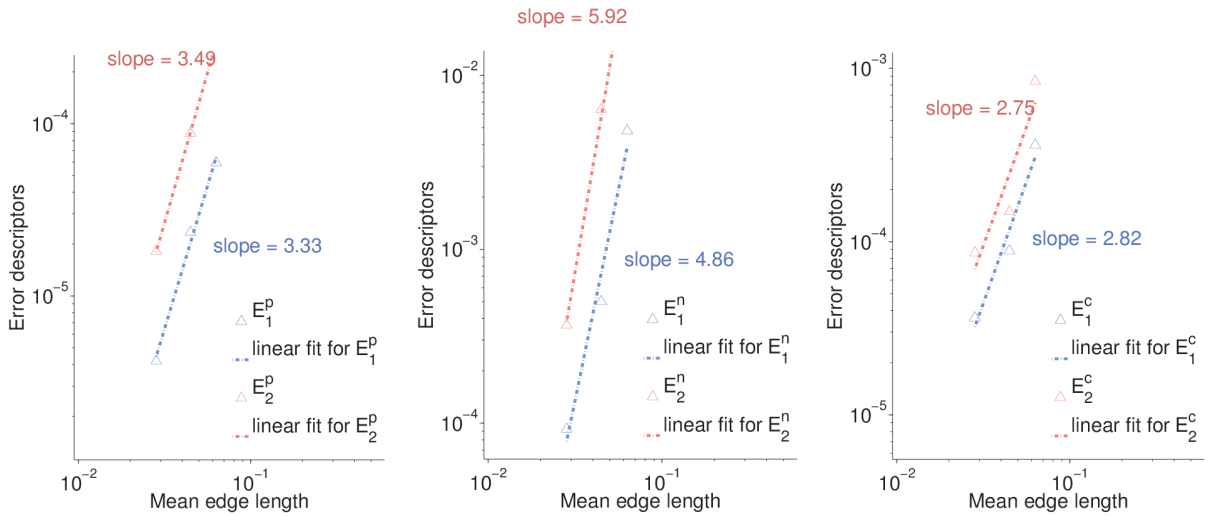


**Figure 9:** *Error vs. mean edge length for the Reuleaux tetrahedron experiment, for positions (left), normals (center) and triple-curves (right).*